CARBON letters

Original Articles
Carbon Letters Vol. 16, No. 2, 127-131 (2015)

Hydrogen storage capacity of highly porous carbons synthesized from biomass-derived aerogels

Yong-Ki Choi and Soo-Jin Park*

Department of Chemistry, Inha University, Incheon 402-751, Korea

Article Info

Received 15 February 2015
Accepted 24 March 2015

***Corresponding Author**
E-mail: sjpark@inha.ac.kr
Tel: +82-32-876-7234

Open Access

DOI: http://dx.doi.org/10.5714/CL.2015.16.2.127

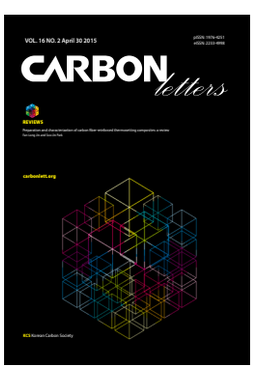

http://carbonlett.org

pISSN: 1976-4251
eISSN: 2233-4998

Abstract

In this work, highly porous carbons were prepared by chemical activation of carbonized biomass-derived aerogels. These aerogels were synthesized from watermelon flesh using a hydrothermal reaction. After carbonization, chemical activation was conducted using potassium hydroxide to enhance the specific surface area and microporosity. The micro-structural properties and morphologies were measured by X-ray diffraction and scanning electron microscopy, respectively. The specific surface area and microporosity were investigated by N_2/77 K adsorption-desorption isotherms using the Brunauer-Emmett-Teller method and Barrett-Joyner-Halenda equation, respectively. Hydrogen storage capacity was dependent on the activation temperature. The highest capacity of 2.7 wt% at 77 K and 1 bar was obtained with an activation temperature of 900°C.

Key words: adsorption, carbon aerogel, hydrogen storage

1. Introduction

Hydrogen has many advantages as an alternative to fossil fuels, as it produces no pollutants, has high energy efficiency, and is essentially an unlimited resource [1-3]. However, its storage presents a problem. Many hydrogen storage methods have been extensively investigated, including metal hybrids, liquid hydrogen, high-pressure hydrogen, and adsorption [4-7]. Among these storage methods, adsorption by carbon materials has many advantages such as good heat resistance, chemical stability, reversibility, and low cost. Many carbon materials for adsorption have also been reported, and include activated carbon, carbon aerogels, graphene, and carbon nanotubes [8-12].

Hydrogen storage capacity is strongly influenced by the specific surface area and microporosity of the adsorbents [13]. Therefore, various methods for the synthesis and surface modification of porous carbons have been developed; for example, templating with other porous materials such as zeolites, metal-organic frameworks (MOFs), and silica [14-17], and direct carbonization of various precursors. Template methods are complicated because they involve the removal of the templated materials. Direct carbonization uses environmentally friendly precursors from agricultural wastes such as rice husks, corncobs, and coconut shells [18,19]. The use of these precursors is also helpful in preventing pollution caused by agricultural wastes. However, biomass-derived carbons (BCAs) have a relatively low specific surface area, and therefore they require activation to increase their specific surface area and micropore volume.

There are two activation methods that are used for BCAs: 1) chemical activation and 2) physical activation [20,21]. Chemical activation is conducted using acidic or basic chemicals such as H_3PO_4, KOH, Na_2CO_3, and NaOH and can lead to high specific surface area and microporosity as a consequence of erosion and oxidation. Physical activation requires an oxidizing gas, such as water vapor, carbon dioxide etc.

In this study, we prepared biomass-derived aerogels from watermelon flesh using a hydrothermal reaction, followed by carbonization. Chemical activation was conducted at various temperatures using KOH to enhance the hydrogen storage capacity of the aerogels.

2. Experimental

2.1. Materials and preparation

Biomass-derived aerogels were prepared by the hydrothermal reaction of watermelon flesh; the details have been provided elsewhere [22]. The watermelon flesh was cut and put into a 100-mL Teflon-lined autoclave. The hydrothermal reaction was conducted at 180°C for 12 h, and then the sample was immersed in a mixture of distilled water and ethanol for several days to remove the impurities. After drying at 80°C for 12 h, the obtained biomass-derived aerogels were carbonized under flowing N_2 (200 mL/min) at 550°C for 1.5 h. The resulting BCA was mixed with KOH (mass ratio of 2), heated to a target temperature in the range 700°C-900°C in a tubular furnace under N_2 atmosphere (200 mL/min), and maintained at the target temperature for 1 h. After cooling down to room temperature, the resulting materials were taken out and washed with distilled water and hydrochloric acid until the pH became neutral. The KOH-activated BCA was labeled K-T-BCA, where T denotes the activation temperature.

2.2. Measurements

X-ray diffraction (XRD) measurements were carried out on a Bruker-AXS D2 Phaser Desktop X-ray Diffractometer with a Lynx-Eye detector using CuKα radiation at 30 kV and 10 mA (λ = 1.5406 Å). The patterns were measured with a scan step time of 3 s and step size of 0.02°. The scanning electron microscope (SEM) images were obtained using Model S-4300SE (Hitachi Co., Ltd.). The textural properties were investigated by nitrogen adsorption-desorption isotherms at -196°C using a gas adsorption analyzer (Model BEL-SORP, BEL Co., Ltd.). The samples were degassed at 200°C for 6 h before the measurement. The hydrogen storage capacity was measured by using a gas adsorption analyzer (Model BEL-SORP, BEL Co., Ltd.) at 77 K and 1 bar. We used ultrahigh purity hydrogen (99.9999%) in order to reduce the influence of other impurities and used the volumetric measurement method to determine the hydrogen storage capacity.

3. Results and Discussion

3.1. Characterization

The XRD patterns of BCA and K-T-BCAs are shown in Fig. 1. They show typical and almost identical carbon peaks. After chemical activation, the peak intensities for carbon at 23° and 44° decreased, because KOH destroys the microstructure of the biomass-derived activated carbons. This mechanism of activation by KOH has been reported previously [23,24] and is summarized below:

$$6KOH + 2C \rightarrow 2K + 3H_2 + 2K_2CO_3 \quad (1)$$

$$K_2CO_3 + C \rightarrow K_2O + 2CO \quad (2)$$

$$K_2O + C \rightarrow 2K + CO \quad (3)$$

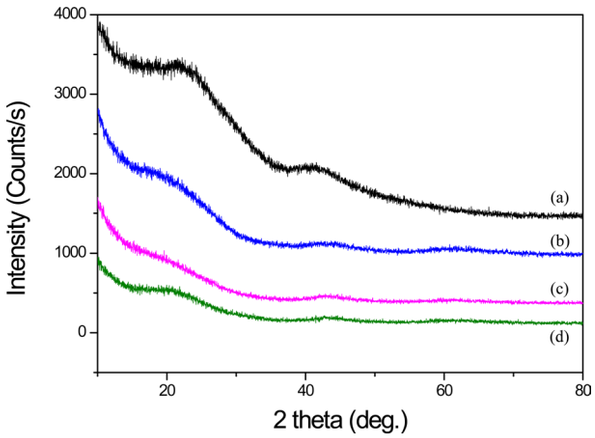

Fig. 1. X-ray diffraction patterns of biomass-derived carbon (BCA) and K-T-BCAs: (a) BCA, (b) K-700-BCA, (c) K-800-BCA, and (d) K-900-BCA.

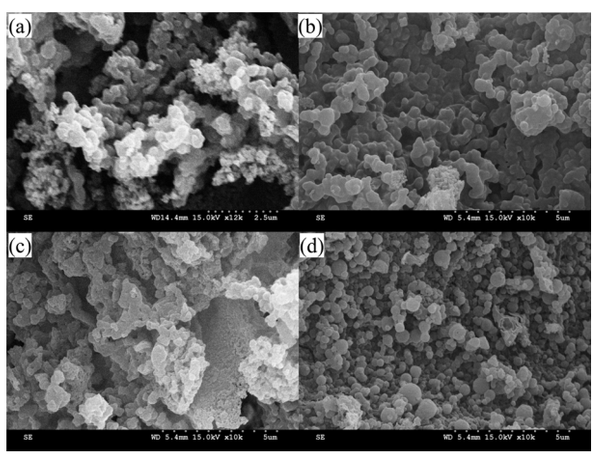

Fig. 2. Scanning electron microscopy images of biomass-derived carbon (BCA) and K-T-BCAs: (a) BCA, (b) K-700-BCA, (c) K-800-BCA, and (d) K-900-BCA.

Potassium is produced during K_2O activation at a high temperature, and it was found that the formation of pores was due to the loss of carbon. The SEM images that are shown in Fig. 2 also indicate the effects of the activation temperature. It can be seen that KOH activation changed the sample particle size and fineness. K-900-BCA has fine particles and regular granules compared with the other K-T-BCAs and BCA. This might be attributed to the erosion of BCAs caused by the higher activation temperature.

Fig. 3 shows the nitrogen adsorption-desorption isotherms at 77 K. BCA and K-T-BCAs appear to have Type 1 isotherms without a noticeable hysteresis loop, which is typical of physisorption in microporous materials [25]. Most of the pores were filled below a relative pressure of about 0.1, indicating that these samples have high microporosity. However, K-800-BCA and K-900-BCA show a slight hysteresis loop and increased adsorption volume of nitrogen at a relative pressure of about 1.0. These results show that the microstructure was destroyed and the macropores were formed at higher activation temperatures.

Fig. 4 shows mesopore and micropore size distributions of BCA and K-T-BCAs. The BCA and K-T-BCAs have similar peaks, but K-900-BCA has the highest peak intensity with most pores <1 nm. Moreover, K-900-BCA shows a relatively high peak intensity above a pore diameter of 50 nm; these results correspond with Fig. 3.

In order to understand the pore structures of the BCA and K-T-BCAs in detail, Table 1 shows the textural properties of BCA and K-T-BCAs. The specific surface area, total pore volume, and micropore volume of K-T-BCAs were influenced by the activation temperature. The specific surface area and pore volume of the samples increase as the activation temperature was increased. As expected, K-900-BCA has the highest specific surface area (1,753 m^2g^{-1}), total pore volume (1.229 cm^3g^{-1}), and micropore volume fraction (72.5%). The high specific surface area and good micropore volume fraction provide good conditions for hydrogen adsorption.

3.2. Hydrogen storage capacities

Fig. 5 shows the hydrogen storage capacities of BCA and K-T-BCAs at 77 K and 1 bar with various sample activation temperatures. K-900-BCA has the highest hydrogen storage capacity of 2.7 wt%. The corresponding values for K-800-BCA, K-700-BCA, and BCA are 2.5, 1.9, and 1.1 wt%, respectively. As can be seen from the results of textural properties, K-900-BCA has the highest specific surface area and micropore volume, and therefore, it has the highest hydrogen storage capacity. These results show that KOH greatly affects carbons at high temperatures. The hydrogen adsorption of the porous carbon materials

Table 1. N_2/77 K textural properties of BCA and K-T-BCAs

Specimens	S_{BET} (m^2/g)	V_{Total} (cm^3/g)	V_{Meso} (cm^3/g)	V_{Micro} (cm^3/g)	V_{Micro} (%)
BCA	419	0.196	0.044	0.152	77.6
K-700-BCA	945	0.404	0.057	0.347	85.9
K-800-BCA	1,428	0.688	0.189	0.499	72.5
K-900-BCA	1,753	1.229	0.547	0.682	55.5

BCA: biomass-derived carbon.
S_{BET}: specific surface area computed using Brunauer-Emmett-Teller equation at a relative pressure range of 0.005-0.04.
V_{Total}: total pore volume is estimated at relative pressure $P/P_0 = 0.99$.
V_{Meso}: mesopore volume determined from the Barrett-Joyner-Halenda equation.
V_{Micro}: micropore volume determined from the subtraction of mesopore volume from the total pore volume.
F_{Micro}: fraction of micropore volume = (micropore volume/total pore volume) × 100.

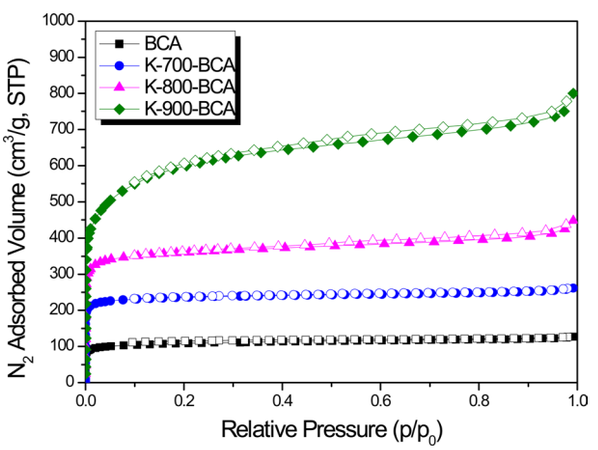

Fig. 3. N_2/77 K adsorption-desorption isotherms of biomass-derived carbon (BCA) and K-T-BCAs.

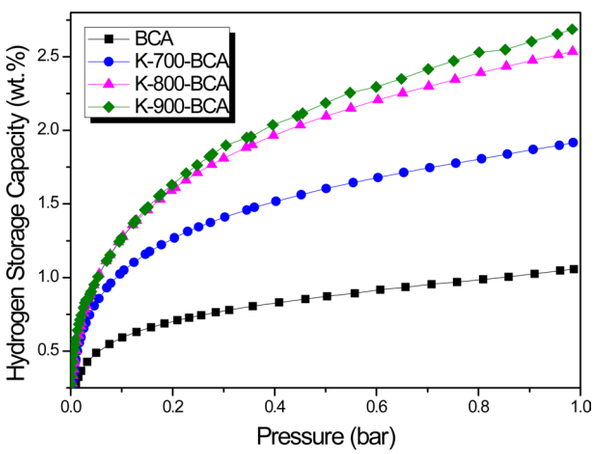

Fig. 5. Hydrogen storage behaviors of biomass-derived carbon (BCA) and K-T-BCAs at 77 K and 1 bar.

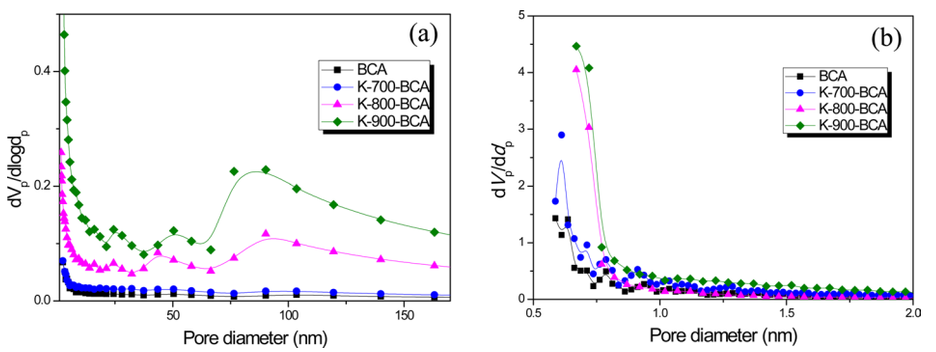

Fig. 4. Mesopore and micropore size distribution of biomass-derived carbon (BCA) and K-T-BCAs.

strongly depended on their microporosity, and the results of these experiments correspond with an earlier report [26]. The hydrogen storage of BCA and K-T-BCAs was also influenced by the microporosity of the samples, which can be enhanced by activation.

4. Conclusions

In this study, we prepared biomass-derived activated carbons using watermelon flesh and a hydrothermal reaction, followed by chemical activation with KOH at various temperatures. The obtained porous carbons had specific surface areas in the range 419-1753 m^2g^{-1} and micropore volumes in the range 0.044-0.547 cm^3g^{-1}. The results show that the specific surface area and micropore volume were influenced by the activation temperature. K-900-BCA showed the highest specific surface area (1753 m^2g^{-1}) and micropore volume (0.547 cm^3g^{-1}). Therefore, K-900-BCA has the highest hydrogen storage capacity, amounting to 2.7 wt% at 77 K and 1 bar. Thus, K-900-BCA can be used as a potential hydrogen storage material and can be enhanced with other metal doping or surface functionalization to increase its hydrogen storage capacity.

Acknowledgments

This work was supported by the Carbon Valley Project by Ministry of Trade, Industry and Energy, Republic of Korea

References

[1] Liu C, Fan YY, Liu M, Cong HT, Cheng HM, Dresselhaus MS. Hydrogen storage in single-walled carbon nanotubes at room temperature. Science, **286**, 1127 (1999). http://dx.doi.org/10.1126/science.286.5442.1127.

[2] Im JS, Park SJ, Kim TJ, Kim YH, Lee YS. The study of controlling pore size on electrospun carbon nanofibers for hydrogen adsorption. J Colloid Sci, **318**, 42 (2007). http://dx.doi.org/10.1016/j.jcis.2007.10.024.

[3] Kim BJ, Lee YS, Park SJ. A study on the hydrogen storage capacity of Ni-plated porous carbon nanofibers. Int J Hydrogen Energy, **33**, 4112 (2008). http://dx.doi.org/10.1016/j.ijhydene.2008.05.077.

[4] Ao Z, Dou S, Xu Z, Jiang Q, Wang G. Hydrogen storage in porous graphene with Al decoration. Int J Hydrogen Energy, **39**, 16244 (2014). http://dx.doi.org/10.1016/j.ijhydene.2014.01.044.

[5] Kim BJ, Lee YS, Park SJ. Novel porous carbons synthesized from polymeric precursors for hydrogen storage. Int J Hydrogen Energy, **33**, 2254 (2008). http://dx.doi.org/10.1016/j.ijhydene.2008.02.019.

[6] Silambarasan D, Surya VJ, Vasu V, Iyakutti K. Single walled carbon nanotubes-metal oxide nanocomposites for reversible and reproducible storage of hydrogen. ACS Appl Mater Interfaces, **5**, 11419 (2013). http://dx.doi.org/10.1021/am403662t.

[7] Jung MJ, Kim JW, Im JS, Park SJ, Lee YS. Nitrogen and hydrogen adsorption of activated carbon fibers modified by fluorination. J Ind Eng Chem, **15**, 410 (2009). http://dx.doi.org/10.1016/j.jiec.2008.11.001.

[8] Robertson C, Mokaya R. Microporous activated carbon aerogels via a simple subcritical drying route for CO_2 capture and hydrogen storage. Microporous Mesoporous Mater, **179**, 151 (2013). http://dx.doi.org/10.1016/j.micromeso.2013.05.025.

[9] Lee SY, Park SJ. Effect of platinum doping of activated carbon on hydrogen storage behaviors of metal-organic frameworks-5. Int J Hydrogen Energy, **36**, 8381 (2011). http://dx.doi.org/10.1016/j.ijhydene.2011.03.038.

[10] Lee SY, Park SJ. Hydrogen storage behaviors of platinum-supported multi-walled carbon nanotubes. Int J Hydrogen Energy, **35**, 13048 (2010). http://dx.doi.org/10.1016/j.ijhydene.2010.04.083.

[11] Lee SY, Park SJ. Preparation and characterization of ordered porous carbons for increasing hydrogen storage behaviors. J Solid State Chem, **184**, 2655 (2011). http://dx.doi.org/10.1016/j.jssc.2011.07.034.

[12] Cho JH, Yang SJ, Lee K, Park CR. Si-doping effect on the enhanced hydrogen storage of single walled carbon nanotubes and graphene. Int J Hydrogen Energy, **36**, 12286 (2011). http://dx.doi.org/10.1016/j.ijhydene.2011.06.110.

[13] Gogotsi Y, Portet C, Osswald S, Simmons JM, Yildirim T, Laudisio G, Fischer JE. Importance of pore size in high-pressure hydrogen storage by porous carbons. Int J Hydrogen Energy, **34**, 6314 (2009). http://dx.doi.org/10.1016/j.ijhydene.2009.05.073.

[14] Yang SJ, Kim T, Im JH, Kim YS, Lee K, Jung H, Park CR. MOF-derived hierarchically porous carbon with exceptional porosity and hydrogen storage capacity. Chem Mater, **24**, 464 (2012). http://dx.doi.org/10.1021/cm202554j.

[15] Lee SY, Park SJ. Synthesis of zeolite-casted microporous carbons and their hydrogen storage capacity. J Colloid Interface Sci, **384**, 116 (2012). http://dx.doi.org/10.1016/j.jcis.2012.06.058.

[16] Cho EA, Lee SY, Park SJ. Effect of microporosity on nitrogen-doped microporous carbons for electrode of supercapacitor. Carbon Lett, **15**, 210 (2014). http://dx.doi.org/10.5714/CL.2014.15.3.210.

[17] Lee SY, Park SJ. A review on solid adsorbents for carbon dioxide capture. J Ind Eng Chem, In press. http://dx.doi.org/10.1016/j.jiec.2014.09.001.

[18] Zhang C, Geng Z, Cai M, Zhang J, Liu X, Xin H, Ma J. Microstructure regulation of super activated carbon from biomass source corncob with enhanced hydrogen uptake. Int J Hydrogen Energy, **38**, 9243 (2013). http://dx.doi.org/10.1016/j.ijhydene.2013.04.163.

[19] Xiao Y, Chen H, Zheng M, Dong H, Lei B, Liu Y. Porous carbon with ultrahigh specific surface area derived from biomass rice hull. Mater Lett, **116**, 185 (2014). http://dx.doi.org/10.1016/j.matlet.2013.11.007.

[20] Hayashi J, Kazehaya A, Muroyama K, Watkinson AP. Preparation of activated carbon from lignin by chemical activation. Carbon, **38**, 1873 (2000). http://dx.doi.org/10.1016/S0008-6223(00)00027-0.

[21] Foo KY, Hameed BH. Preparation of activated carbon by microwave heating of langsat (*Lansium domesticum*) empty fruit bunch waste. Bioresour Technol, **116**, 522 (2012). http://dx.doi.org/10.1016/j.biortech.2012.03.123.

[22] Wu XL, Wen T, Guo HL, Yang S, Wang X, Xu AW. Biomass-derived sponge-like carbonaceous hydrogelsand aerogels for supercapacitors. ACS Nano, **7**, 3589 (2013). http://dx.doi.org/10.1021/nn400566d.

[23] Kim YH, Park SJ. Roles of nanosized Fe_3O_4 on supercapacitive properties of carbon nanotubes. Curr Appl Phys, **11**, 462 (2011).

http://dx.doi.org/10.1016/j.cap.2010.08.018.
[24] Meng LY, Park SJ. Effect of heat treatment on CO_2 adsorption of KOH-activated graphite nanofibers. J Colloid Interface Sci, **352**, 498 (2010). http://dx.doi.org/10.1016/j.jcis.2010.08.048.
[25] Sing KSW. Reporting physisorption data for gas/solid systems with special reference to the determine of surface area and porosity. Pure Appl Chem, **54**, 2201 (2009). http://dx.doi.org/10.1351/pac198254112201.
[26] Chen CH, Huang CC. Hydrogen storage by KOH-modified multi-walled carbon nanotubes. Int J Hydrogen Energy, **32**, 237 (2007). http://dx.doi.org/10.1016/j.ijhydene.2006.03.010.